Single Cell Analysis of Ligand Binding and Complex Formation of Interleukin-4 Receptor Subunits

Thomas Weidemann,[†*] Remigiusz Worch,[†§] Kristina Kurgonaite,[‡] Martin Hintersteiner,[¶] Christian Bökel,[‡] and Petra Schwille[†]

[†]Biophysics Research Group and [‡]Center for Regenerative Therapies Dresden, BIOTEC, Technische Universität Dresden, Dresden, Germany; [§]Institute of Physics, Polish Academy of Sciences, Warsaw, Poland; and [¶]Novartis Institutes for BioMedical Research, Basel, Switzerland

ABSTRACT Interleukin-4 (IL-4) is an important class I cytokine involved in adaptive immunity. IL-4 binds with high affinity to the single-pass transmembrane receptor IL-4Rα. Subsequently, IL-4Rα/IL-4 is believed to engage a second receptor chain, either IL-2Rγ or IL-13Rα1, to form type I or II receptor complexes, respectively. This ternary complex formation then triggers downstream signaling via intracellular Janus kinases bound to the cytoplasmic receptor tails. Here, we study the successive steps of complex formation at the single cell level with confocal fluorescence imaging and correlation spectroscopy. We characterize binding and signaling of fluorescently labeled IL-4 by flow cytometry of IL-4-dependent BaF3 cells. The affinity to ectopically expressed IL-4Rα was then measured by single-color fluorescence correlation spectroscopy in adherent HEK293T cells that express the components of the type II IL-4R but not type I. Finally, IL-4-induced complex formation was tested by dual-color fluorescence cross-correlation spectroscopy. The data provide evidence for codiffusion of IL-4-A647 bound IL-4Rα and the type II subunit IL-13Rα1 fused to enhanced green fluorescent protein, whereas type I complexes containing IL-2Rγ and JAK3 were not detected at the cell surface. This behavior may reflect hitherto undefined differences in the mode of receptor activation between type I (lymphoid) and type II (epithelial) receptor expressing cells.

INTRODUCTION

There is still medical need for improvement in understanding and manipulating cytokine and growth factor signaling (1). Fostered by the continuous expansion and development of new microscopic fluorescence-based methods in the last decade, cell biologists now have access to a broad spectrum of powerful tools to analyze molecular mechanisms at the single cell level (2–4). Within the various approaches to investigate protein-protein interactions in live cells, fluorescence correlation spectroscopy (FCS) is distinguished by providing dynamic information over a broad range of timescales and single-molecule sensitivity (5). With single-color FCS, the molar fractions of molecules with different diffusion properties are temporally resolved. Although changes in molecular mobility are not always large enough for monitoring one-to-one interactions in free solution, the dramatic drop in mobility when binding to the cell membrane makes FCS the ideal tool to study surface receptor binding (6–8).

For most receptor types, ligand binding induces subsequent intermolecular rearrangements within the plasma membrane. Many cytokine receptors form dimers, although higher order oligomers have also been described. Specific interactions between similarly sized proteins can be elegantly assessed with a dual-color extension (fluorescence cross-correlation spectroscopy, FCCS) for which the signal between two spectral channels is cross correlated (9–11). For example, confocal single-point FCCS in cell membranes has been used to detect codiffusion of interleukin-2 receptor α and MHC class I in T-lymphocytes, as well as the existence of preformed dimers for ErbB2 (12,13).

In this study, we use confocal single-color FCS and dual-color FCCS to observe receptor subunits of the interleukin-4 (IL-4) signaling pathway. IL-4R belongs to the class I cytokine receptors, a family of 34 integral single-pass transmembrane proteins (14). In its activated, ligand-bound form, the IL-4 receptor (IL-4R) constitutes a heterodimer, composed of the IL-4Rα chain (CD 124) and either the common γ chain, IL-2Rγ (CD 132; type I IL-4R) or the IL-13Rα1 chain (type II IL-4R) as a coreceptor (15,16). The expression pattern of the two coreceptors reflects their different physiological roles. Type I IL-4R signaling is crucial for the development and maturation of B-cells. In addition, IL-4 is a key cytokine for the differentiation and proliferation of a subset of T-helper cells (Th2), which orchestrate B-cell activation and the production of humoral antibodies. Whereas the type I IL-4R is lymphocyte specific, the type II IL-4R is expressed in epithelia of most other tissues including the brain. Although less is known about the type II function, IL-4 signaling is nevertheless clearly associated with widespread human diseases like asthma, allergy, and atopic dermatitis (17,18).

IL-4 tightly binds the IL-4Rα chain with an affinity of 1–300 pM, whereas the affinity to each coreceptor chain is negligible (19,20). Thus, a sequential binding model was suggested, which could explain why the apparent affinity

Submitted March 31, 2011, and accepted for publication October 11, 2011.

*Correspondence: thomas.weidemann@biotec.tu-dresden.de

Editor: Susan K. Pierce.

0006-3495/11/11/2360/10 $2.00

doi: 10.1016/j.bpj.2011.10.014

of IL-4 measured at the cell surface depends on the surface concentration of coreceptor IL-2Rγ and, more indirectly, why the signaling output increases over the whole range of IL-4 binding (20). The IL-4/IL-4Rα binding interface was thermodynamically mapped with single amino acid resolution (21,22). Recently, crystal structures of the ternary complex of the extracellular domains of IL-4R were reported for both receptor types and ligands (23). However, a direct observation of IL-4-induced ternary complex formation in the plasma membrane of living cells is still lacking.

Here, we present a systematic binding study to fill this gap. First, we produced and characterized a recombinant, fluorescently labeled IL-4 for which we quantified surface binding and proliferation in IL-4-dependent BaF3 cells. Because the small lymphoid cell types are not easily amenable for ectopic expression and single-point confocal FCS, we established adherent HEK293T cells as an experimental platform for binding and oligomerization studies. The affinity of a fluorescently labeled IL-4 to a truncated, signaling deficient IL-4Rα mutant was in good agreement to flow cytometry results obtained in BaF3. Using FCCS revealed that the labeled IL-4-A647 significantly induced cross correlation and thus complex formation with an enhanced green fluorescent protein (eGFP)-tagged IL-13α1 chain, whereas the recruitment of IL-2Rγ was below the detection limit. Our observations challenge the simple cell surface dimerization activation model for type I IL-4R and highlight the importance of observing protein-protein interactions in a native cellular environment. In this regard, we believe that our approach could prove useful to systematically assess other cytokine receptor types as well as disease relevant mutants.

MATERIALS AND METHODS

Protein labeling and analysis

Recombinant human IL-4 (Christian Heuser, Novartis Institutes for BioMedical Research) was randomly labeled with the amino reactive dyes AlexaFluor488 (A488) or AlexaFluor647 (A647) carboxylic acid succinimidyl ester (Invitrogen, Darmstadt, Germany) and purified by gel filtration. Additional details can be found in the Supporting Material.

Gene expression and immunoblotting

Endogenously expressed levels of IL-4R components were analyzed by generating cDNA from isolated HEK293T mRNA, followed by polymerase chain reaction amplification of specific genes. Details for primer design and experimental conditions can be found in the Supporting Material. Proteins were analyzed by SDS-PAGE and immunoblotting. Transfected HEK293T cells were washed with ice cold phosphate-buffered saline and lysed in buffer (25 mM Tris pH 7.2, 150 mM NaCl, 5 mM MgCl2, 0.2% NP-40, 1 mM DTT) containing 5% glycerol and the Complete protease inhibitor cocktail (Roche, Mannheim, Germany). Homogenized lysates were mixed with NuPage sample buffer (Invitrogen) and 100 mM DTT, separated on NuPage 4–12% Bis-Tris gradient gels (Invitrogen) and transferred to a PVDF membrane. Phosphorylated STAT6 protein was detected with a mouse monoclonal antibody (Santa Cruz Biotechnology, Santa Cruz, Ca) followed by a horseradish-peroxidase conjugated secondary antiserum (Sigma, Munich, Germany). Anti-GAPDH (Abcam, Cambridge, UK) was used as an internal control. Horseradish-peroxidase was detected by ECL Plus (Invitrogen) and chemiluminescence quantified with a LAS-3000 imager (Fuji, Düsseldorf, Germany).

Cloning

Using standard methods, we generated cyan, green, and yellow fluorescent protein (eCFP, eGFP, and eYFP) fusion constructs for full-length human IL-4Rα transcription variant 1 (NCBI GI: 56788409) and human IL-2Rγ (NCBI GI:4557881) in the Clontech (Heidelberg, Germany) vector system pEGFP-N1 and its color variants (e.g., pIL4Ra-eGFP-N1). Short versions, e.g., pIL4Ram266-eGFP-N1 that is truncated after 35 amino acids of the cytoplasmic tail, are named after the remaining mature amino acids. Nonfluorescent versions were generated by eGFP excision and religation (e.g., pIL4Ram266-N1). N-terminal hexahistidine tags were added to generate e.g., pNHis-IL4Ra-eGFP-N1. In pNHis-IL4Ram266-eGFP-N1 we removed the initial methionine of the eGFP sequence to suppress cap-independent translation, then named pNHis-IL4-Ram266-eGFP-N2.

Subcloning into pcDNA5/FRT (Invitrogen) yielded pcFRT-NHis-IL4Ram266-eGFP-N2, with which the stable cell line H4G was made. Introducing the early SV40 promoter in pcFRT upstream of the gene yielded a vector system we designated pc2 (24). We introduced IL-13Rα1 (NCBI GI: 26787975), and Fas (CD95, NCBI GI: 23510419) into pc2 and adjusted the expression levels (24). A nonfluorescent version of human JAK3 was expressed by excising eGFP from JAK3-eGFP-N1 (25) and introducing additional stop codons at the C-terminus of the JAK3 (NCBI GI: 189095272). The JAK3 construct lacking the kinase domain (pJAK3dJH1-eGFP-N1) has been described (25). To express human STAT6 (NCBI GI: 23397677) we used pcDNA3.1-GS-STAT6 (Invitrogen). For additional details see the Supporting Material.

Cell culture

For flow cytometry we used a cell line derived from mouse IL-3-dependent pre-B lymphocytes (BaF3, Novartis) (26) that stably expressed human IL-4Rα and IL-13Rα1, conveying growth in response to human IL-4 and IL-13 instead of IL-3. The BaF3 clone used for the proliferation assay stably expressed human IL-4Rα (27). Cells were maintained in RPMI 1640 medium (Gibco) supplemented with 10% serum and 3–6 ng/ml recombinant IL-4 (Novartis). Depletion of IL-4 induced apoptosis within 24 h. Proliferation curves were measured by seeding 1600 cells into 96-well round-bottom plates in RPMI without phenol red containing 10% serum. Cells were stimulated with increasing amounts of recombinant IL-4 (Invitrogen) or IL-4-A647 and evaluated after two days using a luminescent cell viability assay (CellTiter-Glo, Promega, Mannheim, Germany).

pcFRT-NHis-IL4Ram266-EGFP-N2 was introduced into the FRT landing site of the host cell line Flp-In-293 (No. R750-07, Invitrogen) according to the manufacturer's recommendation. Maintenance of Flp-In cells required fibronectin coating of the flasks at 10 μg/ml in phosphate-buffered saline (Becton Dickinson, Heidelberg, Germany), followed by 30 min incubation at 37°C. A stable clone (H4G) was dilution cloned. The IL-4-A647 binding study was carried out in a No. 1.5 borosilicate glass chambered 384-well plate (Matrical, Spokane, WA). Before the experiment the cells were washed and incubated 20 min with increasing concentrations of IL-4-A647 in air buffer (150 mM NaCl, 20 mM Hepes pH7.4, 15 mM Glucose, 46 mM Trehalose, 5.4 mM KCl, 0.85 mM $MgSO_4$, 1.7 mM $CaCl_2$, 0.15 mg/ml bovine serum albumin).

For transient transfections, HEK293T cells were grown in Dulbecco's modified Eagle's medium H21 containing 10% serum and seeded into 8-well chamber slides (LAB-TEK 8-well, Nunc, Langenselbold, Germany).

DNA was transiently transfected using Lipofectamine 2000 (Invitrogen) and OptiMEM-I (Gibco). Cells were observed 24–48 h later in air buffer at 22°C.

Flow cytometry

BaF3 cells were competitively labeled 3–4 days poststimulation using an antibody directed against human IL-4Rα (M57-PE, Becton Dickinson) and IL-4-A488. 7-Actinomycin D (7-AAD; Becton Dickinson) was used for dead cell discrimination and the mouse IgG1 clone MOPC21 as antibody isotype control. Stained cells were measured using a FACSCalibur (Becton Dickinson) flow cytometer. The signal was recorded with logarithmic amplification providing a four-decade log range and plotted as a histogram. The geometric mean of the histogram (fluorescence per cell) was used for calculating the binding curves. All data points were sampled in triplicates. Additional details can be found in the Supporting Material.

Confocal Imaging

Confocal images (see Fig. 2) were taken with a Zeiss Pascal LSM5 (Carl Zeiss, Jena, Germany). The kinetics of IL-4-A647 binding (see Fig. 4) was imaged with avalanche photodiodes on a customized Pickoscreen confocal microscope (PS03, Evotec, Hamburg, Germany) based on the commercial Insight Cell (Perkin Elmer, Waltham, MA). The time-lapsed TIF-images were recorded by an Acapella-based software (MIPS, Evotec) and mean intensities determined using a separate image analysis tool (Optimas, Meyer Instruments, Houston, TX). The area a_1 encompassing the cell comprised three types of pixels: extracellular (*ec*), plasma membrane (*pm*), and cytoplasmic (*cp*), whereas the area a_2 was chosen exclusively extracellular. The mean intensity in a_1 is composed of the concentration of bound or free protein, weighted with the corresponding number of pixels plus background. The ratio

$$\frac{\langle F_1\rangle_{px}}{\langle F_2\rangle_{px}} = \frac{a_2}{a_1}\frac{\left(pm[L_b] + ec\left[L_f\right] + cp[BG]\right)}{\left[L_f\right]} \tag{1}$$

transforms into the linear form B$[L_b]$+C, with B and C as constants for a constant $[L_f]$. The latter condition was fulfilled during the competition experiment (>60 min), for which the data could be represented by a first order exponential decay (Origin Lab, Northampton, MA).

FCS/FCCS

For FCS and FCCS (see Figs. 3 and 5) we used a Zeiss ConfoCor3 system equipped with a C-Apochromat 40× 1.2 W objective. FCS in free solution was evaluated applying a standard 3D diffusion model including a triplet term (9)

$$\begin{aligned} G(\tau) &= \frac{1}{cV_{eff}}G_T(\tau)G_{3D}(\tau) \\ G_T(\tau) &= \left(\frac{1 - f_{nf} + f_{nf}\, e^{-\tau/\tau_{nf}}}{1 - f_{nf}}\right) \\ G_{3D}(\tau) &= \sum_i f_i\left(1 + \frac{\tau}{\tau_{diff,i}}\right)^{-1}\left(1 + \frac{\tau}{S^2\tau_{diff,i}}\right)^{-1/2} \end{aligned}, \tag{2}$$

where f_{nf} and τ_{nf} denote the fraction and time constant of the triplet-dependent decay, and f_i and $\tau_{diff,i}$ the concentration (c) fraction and average dwell time of the particle type i within the illuminated focal volume V_{eff}, respectively. The excitation intensity distribution is assumed to be 3D-Gaussian and stretched along the optical axis by the structure parameter $S = z_0/\omega_0$. If $F/BG < 20$, the average intensity $F_{cor} = F_{tot} - BG$ and the fluctuation amplitude $N_{cor} = (1 + BG/F_{cor})^{-2}\, G^{-1}(\tau)$ were background (BG) corrected and the average counts per particle (CPP), calculated according to CPP = F_{cor}/N_{cor}. Diffusion coefficients and detection volume were derived with a separate measurement of hydrolyzed A488 (D_t = 400 μm^2/s) (28,29) and applying $V_{eff} = S(4\pi D_t\tau_{diff})^{3/2}$.

In cells, we recorded 5 runs for 15 s; runs showing significant intensity changes (>10% changes during the course of the run) were discarded. For pure receptor measurements in the stable cell line H4G, autocorrelations were fitted with $G(\tau) = 1/cV_{eff}G_T(\tau)G_{2D}(\tau)$. The A647-channel was fitted with a combined 3D-2D-diffusion model function

$$\begin{aligned} G(\tau) &= \frac{1}{cV_{eff}}[fG_{3D}(\tau) + (1-f)G_{2D}(\tau)] \\ G_{2D}(\tau) &= \left(1 + \frac{\tau}{\tau_{diff}}\right)^{-1} \end{aligned}, \tag{3}$$

where $G_{3D}(\tau)$, for i = 1, accounted for the freely diffusing ligand in the supernatant. For K_d determination, the fraction of membrane bound ligand was determined. The slightly broadened molecular brightness distribution of labeled IL-4-A647 (2 ± 1.3 dye molecules) was neglected. Assuming a simple 1:1 interaction relates the concentration of bound IL-4-A647 $[L_b] = c\,(1-f)$ to the total concentration of applied ligand

$$\begin{aligned} [L_b] &= \frac{1}{2}\left(A - \sqrt{A^2 - 4[L_t]R_{max}}\right) \\ A &= [L_t] + R_{max} + K_d \end{aligned}, \tag{4}$$

where R_{max} denotes the total concentration of binding sites. Equation (4) was used to calculate the numerical binding isotherm. For K_d determination of the dual-color experiments, we assumed $[L_t] \sim [L_f]$ and computed $K_d = [L_f]([R_{max}] - [L_b])/[L_b]$, where $[R_{max}]$ and $[L_b]$ were expressed in surface density units (μm^{-2}).

For coreceptor recruitment, we used the 3D-2D-diffusion model for both the A647- and the eGFP-channel to account also for trace amounts of freely diffusing eGFP-coupled protein species in the cytoplasm. The particle numbers of the slow component from both channels was then used to calculate the CC ratio (for details see text). Curve fitting was performed with the scripting language Python.

RESULTS AND DISCUSSION

IL-4 in free solution

To observe ligand-receptor interactions, we produced fluorescently labeled, human IL-4. A mild labeling was aimed to preserve the functional integrity of the protein. FCS allowed resolving the relative amounts of free and conjugated dye after purification (see Fig. S2 in the Supporting Material). An average dye-protein stoichiometry of ~1:1 was achieved for IL-4-A488 and 2:1 for IL-4-A647. FCS analysis revealed the absence of protein aggregates after labeling and that the translational diffusion coefficients, with ~100 μm^2/s in aqueous buffer, match well with what can be expected for a 15 kDa protein.

IL-4R-mediated signaling

We first investigated the endogenous content of the IL-4R machinery in the human cell line HEK293T, the cell type we subsequently used for single cell FCS analysis. For

this, cellular mRNA was purified, transcribed into cDNA, and analyzed with gene-specific primers (see Fig. S1). As expected for an epithelial cell line, we identified HEK293T as genuine type II IL-4R expressing cells, with significant bands for the subunits IL-4Rα, JAK1, IL13Rα1, and Tyk2. IL-2Rγ and JAK3 were not detectable while IL-4Rα mRNA expression was very weak. To verify the functionality of the endogenous components, we assayed STAT6 phosphorylation, a hallmark of IL-4R activation (Fig. 1). Because HEK293T cells do not express endogenous STAT6, we therefore transiently overexpressed human STAT6 before stimulation with different amounts and types of ligands (Fig. 1 *A*, *first 4 lanes*). Comparing immunoblot band intensities shows that the activity of randomly labeled IL-4-A647 is attenuated by about 10-fold (Fig. 1 *C*). The concentration of the IL-4-A647 was estimated based on FCS as for single cell binding experiments (see below).

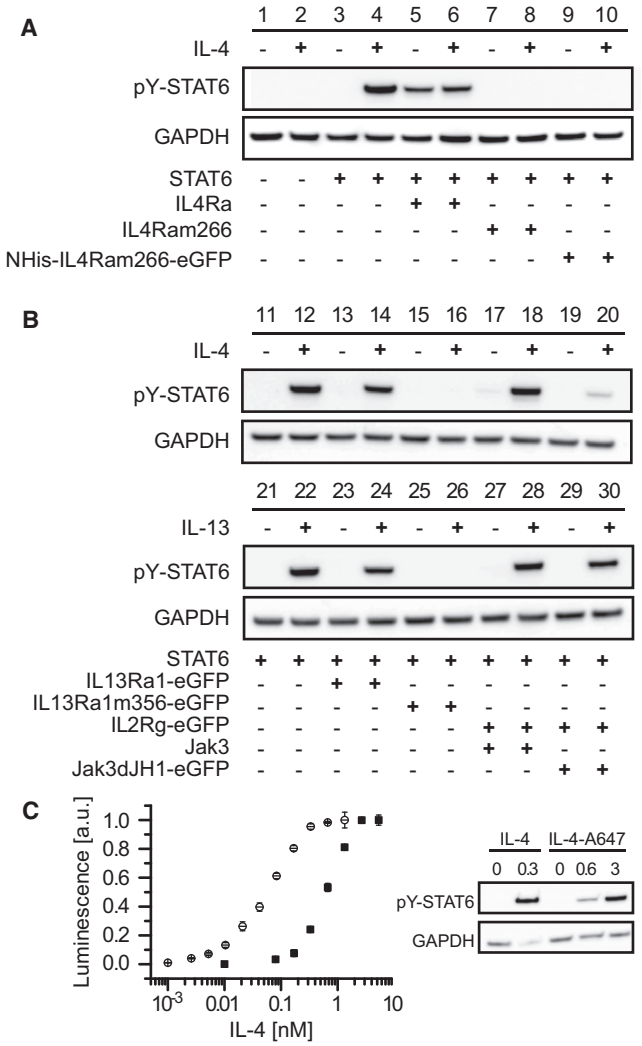

FIGURE 1 IL-4R-mediated signaling. (*A*) Functionality of IL-4R α-chain and (*B*) of coreceptor constructs assayed in HEK293T. Cells were transiently transfected and ligand stimulated (0.6 nM). Pathway activation was detected by phospho-STAT6 immunoblotting; loading control GAPDH. (*C*) Comparison of fluorescently labeled IL-4-A647 with wild-type IL-4. Normalized proliferation curves measured for IL-4-dependent BaF3 and phospho-STAT6 immunoblotting in STAT6 expressing HEK293T.

STAT6 phosphorylation was also used to functionally characterize the different receptor constructs ectopically expressed in HEK293T cells (Fig. 1, *A* and *B*). Transfection of full-length IL-4Rα raises the nonstimulated baseline, indicating signaling function (Fig. 1 *A*, *lane 5*). In contrast, the cytoplasmic deletion construct IL4Ram266 dominantly suppresses endogenous type II signaling, presumably by outcompeting endogenous IL-4Rα for recruitment of IL-13Rα1 into nonfunctional complexes (Fig. 1 *A*, *lanes 8 and 10*). Overexpression of the truncated IL-13 receptor construct IL13Ra1m356-eGFP suppressed type II signaling following stimulation with either IL-4 or IL-13 (Fig. 1 *B*, *lanes 16 and 26*), although overexpression of the full-length, tagged receptor chain IL13Ra1-eGFP did not influence basal signal levels (Fig. 1 *B*, *lanes 13* and *23*).

Cells overexpressing IL2Rg-eGFP and JAK3 were also inducible by IL-4 (Fig. 1 *B*, *lane 18*). However, signal transduction now exclusively occurred via type I complexes, as cotransfection of IL2Rg-eGFP with a JAK3dJH1-eGFP construct lacking the catalytic domain (25) quantitatively suppressed STAT6 phosphorylation (Fig. 1 *B*, *lane 20*). As expected, the type II response following stimulation with IL-13 involving the same endogenous IL-4Rα chains was not affected, neither by the functional nor the dominant negative type I coreceptor (Fig. 1 *B*, *lanes 28* and *30*). Overexpression of the relevant subunits thus allows superimposing the desired type of IL-4R signaling in HEK293T cells.

The different tyrosine phosphorylation sites in the cytoplasmic IL-4Rα chain convey different downstream effects. Whereas phosphorylation of Y575, Y603, Y631 (mature numbering) regulates differentiation via STAT6, IL-4 also acts as a growth factor for lymphoid cells via Y497 and IRS-1 (16). To test the effect of random labeling on cell proliferation, we used IL-4-dependent BaF3 cells that express human IL-4Rα (27,30). These cells were passaged with increasing amounts of nonlabeled IL-4 and fluorescent IL-4-A647 and the cell densities measured two days post-stimulation (Fig. 1 *C*). As for STAT6 phosphorylation, IL-4-A647 exhibited a 10-fold reduced proliferative activity as compared to nonlabeled IL-4. Thus, the changes in ligand activity caused by labeling are equally affecting the different tyrosines in the IL-4Rα tail.

Cell surface binding of IL-4-A488 in BaF3

Native BaF3 cells depend on murine IL-3 for growth (26). The cell line used for the binding studies stably expressed both human type II IL-4R subunits, IL-4Rα, and IL-13Rα1 (Novartis strain), and could thus instead be maintained by IL-4. We passaged the cells under a limiting IL-4

concentration and performed staining after 3 days of resting time. Under these conditions, sufficient ligand-free receptor was accessible at the cell surface to perform binding studies by flow cytometry. The visual appearance of the cells was unchanged, excluding apoptotic effects.

We used the fluorescence per cell readout to generate binding curves and derive K_ds. Staining the cells with increasing concentrations of a phycoerythrin (PE) labeled commercial antibody against the extracellular domain of IL-4Rα (anti-CD124, M57-PE) led to hyperbolic, saturating binding curves (Fig. 2 *A*). The antibody was titrated to estimate the affinity and saturation values. Applying a 1:1 binding model, we obtained for M57-PE an apparent K_d between 5 and 30 nM. Calibrating the signal yielded saturation values between 600 and 2400 receptors per cell (not shown). This magnitude of surface expression levels is in good agreement to similar BaF3 cell lines described in the literature (27).

Titrating IL-4-A488, we always obtained single phase hyperbolic binding curves (Fig. 2 *B*). The dissociation constant for IL-4-A488 was 17 $\pm$ 4 nM, although saturation could not always be fully achieved. This value is two orders of magnitude lower compared to nonlabeled IL-4 (K_d ~150 pM) (27), reflecting the chemical modification and partial inactivation of the protein. Interestingly, we found that the M57 antibody competes with IL-4 for binding to the receptor, facilitating competition experiments to assess the binding specificity of IL-4-A488. M57-PE was efficiently displaced by IL-4-A488, as well as by nonlabeled IL-4 (Fig. 2, *C* and *D*). In the presence of either 7.5 or 10 nM M57-PE, 50% displacement was reached at ~10 nM IL-4-A488. Assuming a 1:1 competition at the binding site, this implies a roughly 10 nM dissociation constant for both labeled ligand and antibody, confirming the affinity range determined from the binding curves. As expected, antibody displacement by nonlabeled IL-4 was more effective than by labeled ligand (Fig. 2 *D*).

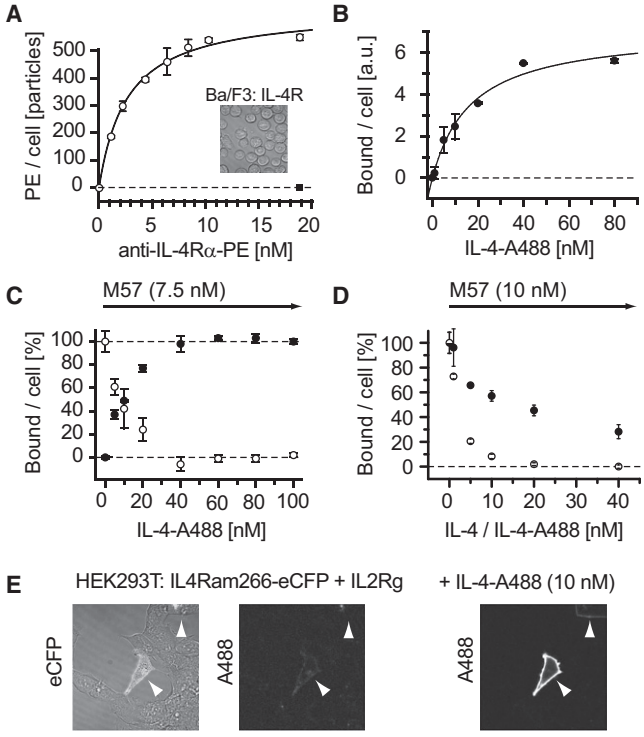

FIGURE 2 Flow cytometry. (*A*) Binding curve of anti-IL-4Rα (M57) to a type II IL-4R expressing BaF3 cell line. Numbers of bound PE per cell were calibrated with fluorescent beads. Isotype control PE-labeled MOPC21 (*solid square*). (*B*) Binding of IL-4-A488 to IL-4R expressing BaF3 (*inset*). (*C*) Simultaneous binding of IL-4-A488 (*solid circles*) and displacement of PE-labeled M57 (*open circles*) measured in the respective color channels. (*D*) Comparative displacement of 10 nM PE-labeled M57 by nonlabeled IL-4 (*open circles*) or IL-4-488 (*solid circles*). (*E*) Confocal images of HEK293T cells transiently expressing type I IL-4R constructs. Imaging with A488 channel before and after administration of IL-4-A488 proves specific binding of the ligand (*arrows*).

Cell surface binding of IL-4-A647 in H4G

Combining microscopic methods with FCS allows for observing cells, receptors, and ligands in real time under quasi-equilibrium conditions. Some minutes after administration of 10 nM IL-4-488, HEK293T cells transiently expressing a shortened, eCFP-tagged version of IL-4Rα and a nonfluorescent IL-2Rγ chain accumulated a seam of A488-fluorescence, whereas the nontransfected neighboring cells remained unstained (Fig. 2 *E*). Thus, binding specificity was sustained in HEK293T. We therefore asked whether it was possible to recapitulate affinity measurements of the labeled ligand in HEK293T by FCS. This would provide a platform for single cell, single molecule analysis of IL-4R complex formation that cannot easily be performed in lymphocytes.

We chose eGFP for tagging of receptor chains, because it is a well-established fluorophore for in vivo FCS applications and can be combined with IL-4-A647 for dual-color applications. For convenient cell handling, we created a stable cell line (H4G) expressing NHis-IL4Ram266-eGFP, a tagged and truncated IL-4Rα retaining only 35 cytoplasmic amino acids before the eGFP (native tail length is 569 amino acids). The truncated tail still contains the box1 motif that promotes JAK1 binding (not shown). Unlike the full-length receptor, at steady state these constructs largely accumulate at the plasma membrane (Fig. 3B) in a comparably narrow concentration range (Fig. S4).

For the ligand binding study, H4G cells were incubated with increasing amounts of IL-4-A647. Cross sections show ligand freely diffusing in the extracellular space, as well as bound to the plasma membrane (Fig. 3 *B*). During the experiment, some of the ligand was internalized and appeared in small vesicles; however the uptake was very slow. At 22°C, cells could be measured for 2 h without significant interference by internalized A647 fluorescence. FCS was performed following a park-and-probe sequence: The cross

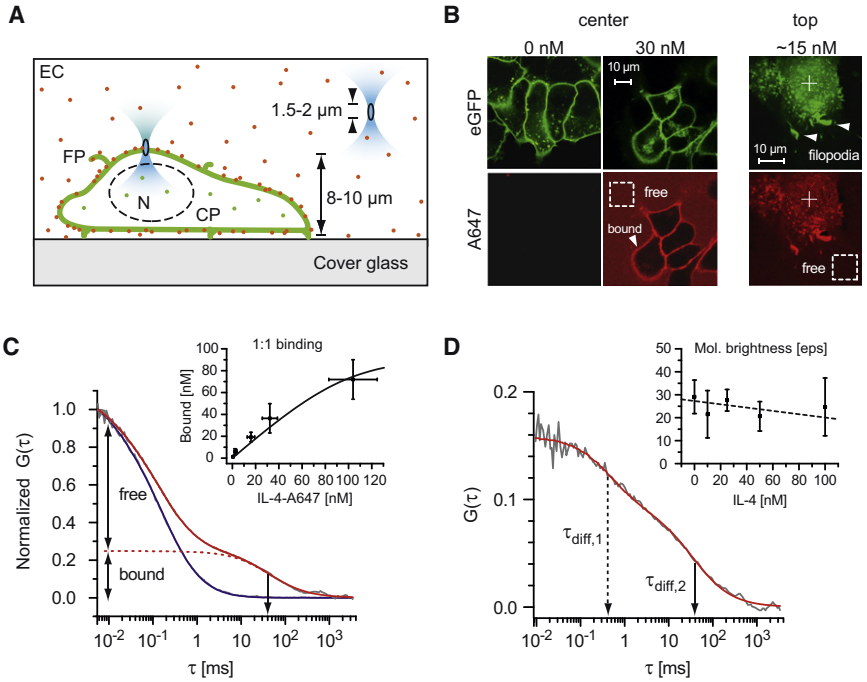

FIGURE 3 Single-color FCS on the cell surface. (*A*) Dimensions of the detection volume as positioned in free solution or at the apical membrane. Above the nucleus (N), fluorescence from filopodia (FN), the extracellular compartment (EC), and the cytoplasm (CP) may also be detected. (*B*) Confocal cross sections of the stable cell line H4G in the absence or presence of ligand IL4-A647. A typical position for single-point FCS is indicated at the top (*cross hair*). (*C*) Normalized correlation curves (*data gray*) measured in the supernatant (*blue*) and at the top of the apical membrane (*red*). Binding isotherm (*inset*) obtained by evaluating the molar fractions with a numerical example assuming 1:1 binding (K_d = 10 nM, R_{max} = 100 nM). (*D*) Receptor diffusion. Correlation curve (*data gray*) and fitting with two correlation times (*red*, *arrows*). The molecular brightness of the eGFP-tagged receptors for saturating IL-4 binding as measured by the photon counting histogram (*inset*).

section of the cells was scanned at z = 3–6 μm distances from the glass surface. At this height, the optical axis was positioned in the middle of the nucleus. The laser focus was then moved toward the apical membrane via the objective drive to z = 8–10 μm (see also Fig. 3 *A*). From the eGFP-channel, we obtained a diffusion coefficient of D_t = 0.4 ± 0.11 $\mu m^2/s$ and a chromophore blinking time of τ_{nf} = 490 ± 200 μs. Both the diffusion coefficient of the receptors and the blinking time fall in the expected range for a membrane anchored, eGFP-tagged single-pass transmembrane protein (31,32).

An example correlation curve for the ligand IL-4-A647 in the apical membrane is shown in Fig. 3 *C*. Compared to the fast decay, as measured in free solution, membrane binding produces a pronounced second component with a correlation time of the same order of magnitude as determined for the receptor in the eGFP-channel (Fig. 3 *D*). Using a combined 3D-2D two-component model (Eq. 3), the molar fractions of bound ligand (f_2) can be derived from the fit and, in principle, be used to calculate a binding curve. Based on the eGFP channel, the average 2D receptor density in our cells was 56 ± 25 μm^{-2}, which is equivalent to an apparent 3D concentration of ~100 nM within the focal volume. Because FCS measurements are limited to nanomolar concentrations of fluorescent particles, saturation could not be reached, and an accurate K_d could not be derived by fitting model functions. However, assuming the same molecular brightness for IL-4-A647 in its different states and a simple one-to-one binding model, a receptor concentration of 100 nM and K_d = 10 nM adequately represents the data (Fig. 3 *C*, *inset*). In addition, dual-color autocorrelation measurements allow evaluating the occupied receptor fraction and the K_d for each individual cell. With an average K_d =15 ± 8 nM, the affinity between labeled IL-4 and IL-4Rα was in good agreement with the values obtained by flow cytometry.

Diffusion and binding of IL-4-A647 is sufficiently slow such that surface binding could be followed by time-lapse imaging (Fig. 4 *A*). For a kinetic experiment, a receptor-expressing cell was selected in the eGFP-channel. Ligand was carefully added in a small volume (1/10), such that the image of the cell was kept in place and could be monitored in the A647-channel. The slow diffusion-driven expansion into the supernatant led to a successive increase of intensity, first in the extracellular space and later, due to receptor binding, at the plasma membrane. In Fig. 4 *B*, we plotted the mean intensity of a region of interest encompassing the cell, normalized by a second region of interest selected in the supernatant; under certain assumptions, this ratio is proportional to the concentration of bound ligand (Eq. 1). After some delay (15 min), this ratio increased linearly, and reached its maximum after 40 min, followed by a slight decrease to a stable plateau. Adding a 10-fold excess of unlabeled IL-4 initiated competition of the labeled by the nonlabeled IL-4. From 80 min upward, the concentration of bound ligand followed closely a first order exponential decay. The time constant t = 5.4 min directly relates to the inverse off-rate $k_{off} = 3 \times 10^{-3}\ s^{-1}$, which is in good agreement with in vitro off-rates determined by surface plasmon resonance ($k_{off} = 2.1 \times 10^{-3}\ s^{-1}$ (21)). Therefore, the decrease in affinity for labeled relative to nonlabeled IL-4 must reflect a reduction of the on-rate.

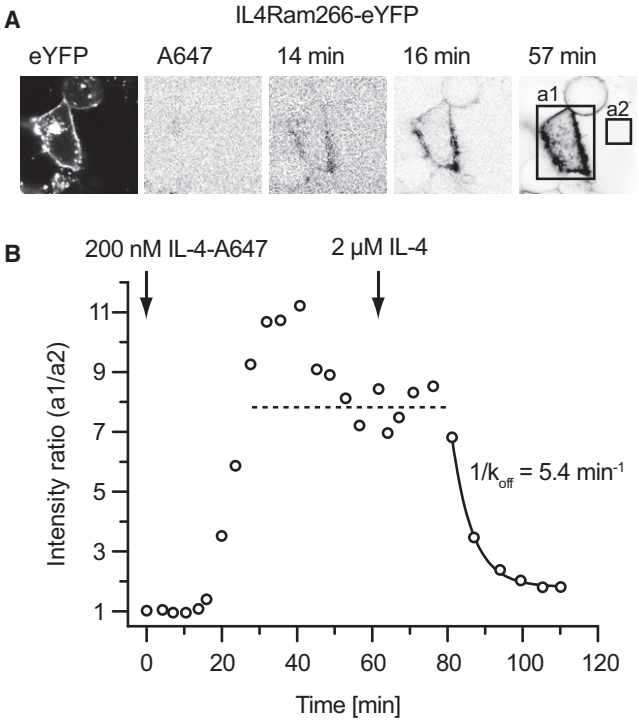

FIGURE 4 Single-cell binding kinetics in HEK293T. (*A*) Confocal cross sections of a HEK293T cell transiently expressing IL-4Ram266-eYFP successively binding the ligand IL-4-A647 (eYFP and A647 channels in *gray scale*). (*B*) Time course of the ratio of mean intensities obtained from the images in the area a_1 and a_2. Administration of ligand IL-4-A647 and competition wild-type IL-4 at indicated concentrations and time points.

According to the crystal structure (Fig. S3), four out of 12 primary amino groups (11 lysines plus N-terminus) of IL-4 locate close to the IL-4Rα binding interface (K12, K61, K77, and K84), where labeling would directly interfere with binding. At an average of two dye labels per IL-4, roughly 40% of IL-4 molecules should not be affected. The strong reduction in affinity must be accounted for by different mechanisms, e.g., by effects of the negatively charged dyes on the electrostatic steering thought to underlie the unusually high on-rate in IL-4 binding (21).

The transient maximum in the binding kinetics could indicate receptor oligomerization. Assuming fast initial binding, a shared ligand would lead to a subsequent slow decrease in the concentration of bound ligand. Because IL-4Rα homodimer-mediated signaling has been proposed (33), we tested ligand-induced homotypic interactions of the IL-4Rα chains with the photon counting histogram approach (34). We found that the molecular brightness of eGFP-tagged receptors in the plasma membrane of H4G cells was unchanged up to very high IL-4 concentrations (Fig. 3 *D*, *inset*), excluding significant ligand-induced receptor oligomerization in the plasma membrane. We therefore suppose that the transient maximum is rather a result of phase shifts in the underlying kinetic reactions. For the initial phase, in which the concentration of membrane bound IL-4 rises linearly, it can be assumed that all the ligands approaching the cell surface are immediately bound, while equilibrium with dissociating molecules is not yet fully established.

IL-4-A647-induced coreceptor recruitment in HEK293T

After ligand binding, the next crucial event in IL-4R activation is ternary complex formation of IL-4/IL-4Rα and either of the two coreceptor chains. We therefore asked whether labeled IL-4 could recruit the different eGFP-tagged receptor chains into a complex (Fig. 5 *A*). Working with a labeled ligand has the advantage that one can track and quantify binding to the particular cell under study. We applied dual-color FCCS to measure the fraction of complexes carrying A647 coupled to the ligand and eGFP coupled to the coreceptor. The approach required transient coexpression of a nonfluorescent IL-4Rα chain (NHis-IL4-Ram266) with an eGFP-tagged coreceptor chain. Labeled IL-4 bound to the NHis-IL4Ram266-eGFP positive control provided the maximum achievable cross-correlation amplitude for the current alignment. To define the baseline we used an eGFP-tagged version of the death receptor Fas (CD95), not related to the IL-4 signaling pathway. Surface partitioning of IL-2Rγ at sufficient levels for FCS required coexpression of nonfluorescent JAK3 that, like other JAKs, act as a chaperone for endoplasmic reticulum export of the associated receptor (35) but, like IL-2Rγ is not normally expressed in HEK293T cells (Fig. S1 (25)).

Applying IL-4-A647 at concentrations slightly above K_d (~20–50 nM) led to quantitative binding. Confocal images of cells selected for FCCS expressing combinations of a nonfluorescent, ligand binding α-chain with different eGFP-tagged coreceptors were visually similar (Fig. S5). We selected cells where a large fraction of the receptors showed quantitative colocalization at the plasma membrane, and the plasma membrane distributions appeared spatially homogenous. The transiently transfected cells exhibited a broad distribution of expression levels. As judged from the autocorrelation amplitudes in the eGFP-channel, we measured cells with on average ~200 eGFP receptors per μm^2 in the plasma membrane, covering the broad range of 30–680 receptors per μm^2. The correlation curves measured in transiently transfected cells contained slightly different correlation times as compared to NHis-IL4Ram266-eGFP in the stable cell line H4G: The fast correlation time was shifted up to the lower millisecond regime with a persistent molar fraction of ~30%. We think this cannot be due to chromophore blinking but rather represents a combination of blinking and trace amounts of eGFP-tagged protein species freely diffusing in the cytoplasm. Indeed, some of the cells showed a faint background of diffuse intensity in confocal cross sections. Either proteolysis or escape from initial AUG translation initiation may be an underlying biological

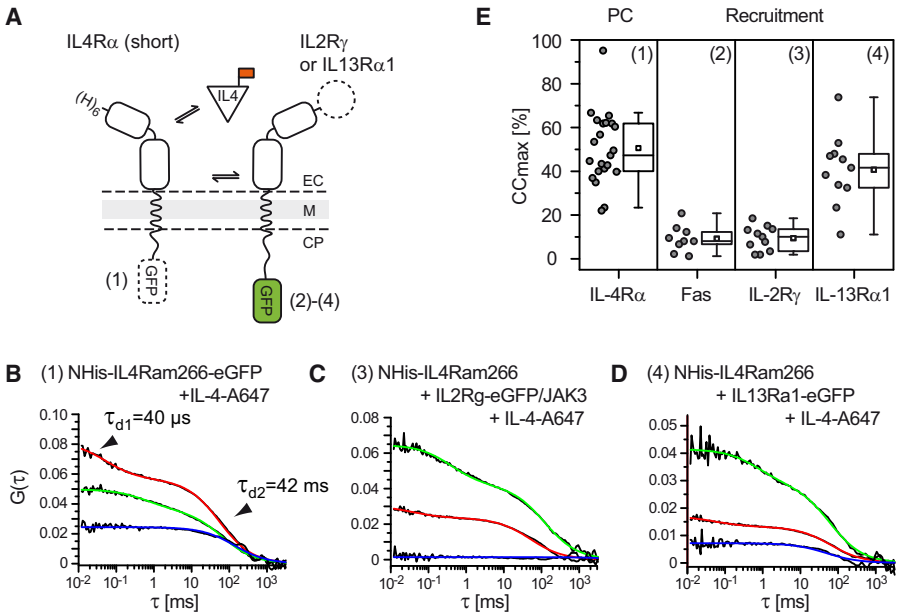

FIGURE 5 Coreceptor recruitment of IL-4-A647. (*A*) Schematic IL-4R subunits as used for single-cell analysis in the plasma membrane (EC, extracellular; M, membrane; CP, cytoplasm). As a positive control (PC), a short eGFP-tagged IL-4Rα chain was expressed (1). For coreceptor recruitment, the eGFP was transferred to either Fas (2), IL-2Rγ (3), or IL-13Rα1 (4). (*B–D*) Correlation curves (*data gray*) recorded by top positioning in transiently transfected HEK293T cells stained with IL-4-A647. Fitting curves for eGFP (*green*), A647 (*red*), and the cross-correlation channel (*blue*) as simultaneously measured. (*E*) The maximum ratio of cross- and autocorrelation (CC_{max}) plotted for individual cells (*solid circles*) and summarized in percentiles defined by the mean $\pm 25\%$ (*box*), $\pm 75\%$ (*ticks*), and the median (*small, open square*).

reason (36). To cope with a freely diffusing species, we evaluated channels, eGFP and A647, with the 3D1C-2D1C diffusion model. For the positive control NHis-IL4-Ram266-eGFP we obtained with $D_{t2} = 0.13 \pm 0.08$ $\mu m^2/s$ a somewhat smaller value than in the stable H4G cell line; the difference is most likely attributed to the alternate fitting model. The other eGFP-tagged receptors ranged between 0.1 and 0.3 $\mu m^2/s$.

FCCS in dual-color mode produces three correlation curves, one for each color channel and the cross-correlation curve (Fig. 5, *B–D*). We evaluated the membrane-bound particle numbers for the eGFP, the A647, and the cross-correlation channel (N_g, N_r, and N_{gr}) by fitting. The fraction of formed complexes was determined as the ratio designated $CC_g = N_{gr}/N_g$ or $CC_r = N_{gr}/N_r$. Due to asymmetric expression levels either more red or more green particles are in the observation volume, therefore one of the CC values is always larger for the same number of formed complexes. To minimize this bias, we always took the maximum CC (either CC_g or CC_r) as a representative value for the particular cell (designated CC_{max}). For NHis-IL4Ram266-eGFP (positive control) we measured $CC_{max} = 51 \pm 17\%$ and for the FasR-eGFP (negative control) $CC_{max} = 9 \pm 6\%$. Having the experimental range defined, we obtained for IL2Rg-eGFP $CC_{max} = 9 \pm 6\%$ and for IL13Ra1-eGFP $CC_{max} = 41 \pm 17\%$. Thus, whereas ligand-mediated IL-2Rγ recruitment into the ternary complex was indistinguishable from the negative control; IL-4-A647-dependent recruitment of IL-13Rα1 was significant (Fig. 5 *E*).

How can the drastic difference of the measured cross-correlation levels for the two IL-4R types be explained? One possibility is that the newly formed type I complexes are cleared from the membrane so rapidly that they become undetectable before the background of freely diffusing subunits. Because we observe the receptors under steady state with continued presence of ligand, clearance due to endocytosis would have to be a much faster process than complex formation. However, a significant internalization during the course of the experiment is not supported by our observations, as we did not observe a large accumulation of fluorescent ligand or truncated, eGFP-tagged receptors in the cytoplasm of the cells. Another possibility is selective bleaching of type I complexes in the focal volume. Immobilization of IL-2Rγ/JAK3 may be mediated by ligand-induced interactions with the cytoskeleton, for example the actin cortex (32). However, we did not observe a pronounced bleaching of eGFP-tagged receptors in the presence of ligand. Finally, chemical labeling might reduce the affinity such that the type I complex lifetime becomes too short with respect to the diffusion times (<90 ms). It is conceivable that binding at the cell surface selects IL-4-A647 species for which the dyes have been attached distant to the IL-4Rα binding interface. From these eight accessible amino groups, only K126 seems to be sterically involved in the IL-2Rγ binding (Fig. S3). Recalling that two dye molecules were on average conjugated to IL-4-A647, ~75% of the ligands should not be labeled at K126. However, for IL13-Rα1, the CC-values reached in average as much as 80% of the positive control; a small reduction as compared to the 100-fold loss in apparent surface affinity toward IL-4Rα. The data therefore instead suggest a much lower affinity toward IL-2Rγ—such that the fraction of formed complexes remains below the detection threshold for our FCCS approach.

CONCLUSIONS

Here we analyze, to our knowledge for the first time, fluorescently tagged IL-4 receptor subunits with single

molecule resolution in living cells. The surface affinity of labeled IL-4 was determined with flow cytometry and single-color FCS. The results were remarkably consistent despite the fact that the surface receptor densities in the murine, lymphoid BaF3 cells were rather physiological, whereas ectopic overexpression in epithelial HEK293T cells produced three to four orders of magnitude higher values. Chemical labeling of IL-4 reduced the binding affinity about 100-fold. In contrast, downstream signaling activity was reduced by a factor of 10-fold, as independently assayed by STAT6 phosphorylation and IRS1/2-dependent proliferation. Thus, the IL-4R signaling machinery translates the loss in ligand affinity with a smaller conversion factor, indicating that a subnanomolar affinity is not a stringent prerequisite for generating a full signaling response (20).

A key step for signal transduction is the cross activation of JAKs bound to the receptor's cytoplasmic tails. It is generally believed that ligand-induced dimerization is necessary to bring the JAKs into a signaling productive spatial orientation (37). We recently showed in membrane blebs that neither IL-4Rα nor IL-2Rγ have a propensity to exist as preformed dimers (24). Therefore, ligand binding must, at some stage in the cascade, drive complex formation. We assayed IL-4-A647 for its activity to induce dimerization by dual-color FCCS. To our surprise, we failed to detect recruitment of IL-2Rγ, whereas dimerization with IL-13Rα1 was almost in saturation. These observations imply that the affinity for the two coreceptor subtypes differ dramatically, contrasting biochemical studies using recombinantly expressed extracellular domains (23). We conclude that the cytoplasmic portions of the receptors in conjunction with the membrane environment in living cells have significant impact on the binding thermodynamics. Whereas for type II signaling the data are in agreement with the canonical ligand-induced dimerization model, the behavior of type I receptor subunits is rather intriguing and calls for further investigations.

SUPPORTING MATERIAL

Additional details, a table, five figures, and references are available at http://www.biophysj.org/biophysj/supplemental/S0006-3495(11)01204-5.

We thank Peter Krammer (German Cancer Research Center, Heidelberg, Germany) for providing the CD95 sequence, Sigrun Hofmann (Children's Hospital, TU Dresden, Dresden) for providing JAK3 constructs, and Attila Szanto and Lazlo Nagy (Medical and Health Science Center, University of Debrecen, Debrecen, Hungary) for providing STAT6. We thank Karin Crell, Ellen Sieber, Sarah Herrmann, Sabine Knappe, Stephanie von Kannen, and Raquel Palencia for their committed technical assistance.

R.W. is grateful for receiving a postdoctoral fellowship from the Alexander von Humboldt Foundation (Germany). The use of a Confocor3 was amply supported by Carl Zeiss AG (Jena, Germany). C.B., P.S., and T.W. received a Center of Regenerative Medicine Dresden seed grant Development of reporter constructs for the live imaging of Jak/Stat signaling.

REFERENCES

1. Whitty, A., and T. V. Riera. 2008. New ways to target old receptors. *Curr. Opin. Chem. Biol.* 12:427–433.
2. Briddon, S. J., and S. J. Hill. 2007. Pharmacology under the microscope: the use of fluorescence correlation spectroscopy to determine the properties of ligand-receptor complexes. *Trends Pharmacol. Sci.* 28:637–645.
3. Lidke, D. S., and B. S. Wilson. 2009. Caught in the act: quantifying protein behaviour in living cells. *Trends Cell Biol.* 19:566–574.
4. Liu, P., S. Ahmed, and T. Wohland. 2008. The F-techniques: advances in receptor protein studies. *Trends Endocrinol. Metab.* 19:181–190.
5. Kim, S. A., K. G. Heinze, and P. Schwille. 2007. Fluorescence correlation spectroscopy in living cells. *Nat. Methods.* 4:963–973.
6. Briddon, S. J., R. J. Middleton, …, S. J. Hill. 2004. Quantitative analysis of the formation and diffusion of A1-adenosine receptor-antagonist complexes in single living cells. *Proc. Natl. Acad. Sci. USA.* 101:4673–4678.
7. Meissner, O., and H. Häberlein. 2003. Lateral mobility and specific binding to GABA(A) receptors on hippocampal neurons monitored by fluorescence correlation spectroscopy. *Biochemistry.* 42:1667–1672.
8. Rigler, R., A. Pramanik, …, J. Wahren. 1999. Specific binding of proinsulin C-peptide to human cell membranes. *Proc. Natl. Acad. Sci. USA.* 96:13318–13323.
9. Bacia, K., S. A. Kim, and P. Schwille. 2006. Fluorescence cross-correlation spectroscopy in living cells. *Nat. Methods.* 3:83–89.
10. Schwille, P., F. J. Meyer-Almes, and R. Rigler. 1997. Dual-color fluorescence cross-correlation spectroscopy for multicomponent diffusional analysis in solution. *Biophys. J.* 72:1878–1886.
11. Weidemann, T., M. Wachsmuth, …, J. Langowski. 2002. Analysis of ligand binding by two-colour fluorescence cross-correlation spectroscopy. *Single Mol.* 3:49–61.
12. Vámosi, G., A. Bodnár, …, S. Damjanovich. 2004. IL-2 and IL-15 receptor alpha-subunits are coexpressed in a supramolecular receptor cluster in lipid rafts of T cells. *Proc. Natl. Acad. Sci. USA.* 101:11082–11087.
13. Liu, P., T. Sudhaharan, …, T. Wohland. 2007. Investigation of the dimerization of proteins from the epidermal growth factor receptor family by single wavelength fluorescence cross-correlation spectroscopy. *Biophys. J.* 93:684–698.
14. Boulay, J. L., J. J. O'Shea, and W. E. Paul. 2003. Molecular phylogeny within type I cytokines and their cognate receptors. *Immunity.* 19:159–163.
15. Hershey, G. K. 2003. IL-13 receptors and signaling pathways: an evolving web. *J. Allergy Clin. Immunol.* 111:677–690, quiz 691.
16. Nelms, K., A. D. Keegan, …, W. E. Paul. 1999. The IL-4 receptor: signaling mechanisms and biologic functions. *Annu. Rev. Immunol.* 17:701–738.
17. Lloyd, C. M., and E. M. Hessel. 2010. Functions of T cells in asthma: more than just T(H)2 cells. *Nat. Rev. Immunol.* 10:838–848.
18. Romagnani, S. 2000. The role of lymphocytes in allergic disease. *J. Allergy Clin. Immunol.* 105:399–408.
19. Miloux, B., P. Laurent, …, P. Ferrara. 1997. Cloning of the human IL-13R alpha1 chain and reconstitution with the IL4R alpha of a functional IL-4/IL-13 receptor complex. *FEBS Lett.* 401:163–166.
20. Whitty, A., N. Raskin, …, L. C. Burkly. 1998. Interaction affinity between cytokine receptor components on the cell surface. *Proc. Natl. Acad. Sci. USA.* 95:13165–13170.
21. Wang, Y., B. J. Shen, and W. Sebald. 1997. A mixed-charge pair in human interleukin 4 dominates high-affinity interaction with the receptor alpha chain. *Proc. Natl. Acad. Sci. USA.* 94:1657–1662.
22. Zhang, J. L., I. Simeonowa, …, W. Sebald. 2002. The high-affinity interaction of human IL-4 and the receptor alpha chain is constituted by two independent binding clusters. *J. Mol. Biol.* 315:399–407.

23. LaPorte, S. L., Z. S. Juo, …, K. C. Garcia. 2008. Molecular and structural basis of cytokine receptor pleiotropy in the interleukin-4/13 system. *Cell.* 132:259–272.

24. Worch, R., C. Bökel, …, T. Weidemann. 2010. Focus on composition and interaction potential of single-pass transmembrane domains. *Proteomics.* 10:4196–4208.

25. Hofmann, S. R., A. Q. Lam, …, J. J. O'Shea. 2004. Jak3-independent trafficking of the common gamma chain receptor subunit: chaperone function of Jaks revisited. *Mol. Cell. Biol.* 24:5039–5049.

26. Palacios, R., G. Henson, …, J. P. McKearn. 1984. Interleukin-3 supports growth of mouse pre-B-cell clones in vitro. *Nature.* 309:126–131.

27. Deutsch, H. H., K. Koettnitz, …, F. S. Kalthoff. 1995. Distinct sequence motifs within the cytoplasmic domain of the human IL-4 receptor differentially regulate apoptosis inhibition and cell growth. *J. Immunol.* 154:3696–3703.

28. Dertinger, T., V. Pacheco, …, J. Enderlein. 2007. Two-focus fluorescence correlation spectroscopy: a new tool for accurate and absolute diffusion measurements. *ChemPhysChem.* 8:433–443.

29. Kapusta, P. 2010. Absolute Diffusion Coefficients: Compilation of Reference Data for FCS Calibration. Application Note. PicoQuant GmbH, Berlin, Germany.

30. Koettnitz, K., and F. S. Kalthoff. 1993. Human interleukin-4 receptor signaling requires sequences contained within two cytoplasmic regions. *Eur. J. Immunol.* 23:988–991.

31. Haupts, U., S. Maiti, …, W. W. Webb. 1998. Dynamics of fluorescence fluctuations in green fluorescent protein observed by fluorescence correlation spectroscopy. *Proc. Natl. Acad. Sci. USA.* 95:13573–13578.

32. Pillet, A. H., V. Lavergne, …, T. Rose. 2010. IL-2 induces conformational changes in its preassembled receptor core, which then migrates in lipid raft and binds to the cytoskeleton meshwork. *J. Mol. Biol.* 403:671–692.

33. Fujiwara, H., S. H. Hanissian, …, R. S. Geha. 1997. Homodimerization of the human interleukin 4 receptor alpha chain induces Cepsilon germline transcripts in B cells in the absence of the interleukin 2 receptor gamma chain. *Proc. Natl. Acad. Sci. USA.* 94:5866–5871.

34. Chen, Y., L. N. Wei, and J. D. Müller. 2003. Probing protein oligomerization in living cells with fluorescence fluctuation spectroscopy. *Proc. Natl. Acad. Sci. USA.* 100:15492–15497.

35. Huang, L. J., S. N. Constantinescu, and H. F. Lodish. 2001. The N-terminal domain of Janus kinase 2 is required for Golgi processing and cell surface expression of erythropoietin receptor. *Mol. Cell.* 8:1327–1338.

36. Kozak, M. 1999. Initiation of translation in prokaryotes and eukaryotes. *Gene.* 234:187–208.

37. Weidemann, T., S. Höfinger, …, M. Auer. 2007. Beyond dimerization: a membrane-dependent activation model for interleukin-4 receptor-mediated signalling. *J. Mol. Biol.* 366:1365–1373.